

Hard Carbon Derived from Straw as Anode Materials for Sodium-ion Batteries

Hua-zhi Zhang^{1,*}, Chao Chen¹, Hui Xu², Li-wen Yang³, Jian Chen⁴

¹ College of Applied Chemical Engineering, Sichuan Vocational College of Chemical Technology, Luzhou, 646000, China

² School of Materials and Chemical Engineering, Shanghai Institute of Technology, Shanghai, 201418, China

³ School of Chemical Engineering, Sichuan University, Chendu, 610020, China

⁴ School of Materials and Chemical Engineering, Sichuan University of Science and Engineering, Zigong, 643002, China

*E-mail: iwontgiveup@126.com

Received: 12 July 2022 / Accepted: 8 September 2022 / Published: 10 October 2022

In recent years, sodium-ion batteries have been widely concerned due to their low price and rich natural resources, and are considered to replace the next generation of energy storage materials for lithium-ion batteries. Straw obtains the carbon electrode as the sodium ion battery anode material through simple carbonize. Using straw as the precursor, we prepared a hard carbon electrode material with fluffy porous structure and rich cellulose / hemicellulose through a simple carbonize method, which was completely decomposed and left without carbon residue or converted into high graphitic carbon during carbonize. Through characterization and electrochemical analysis, we found that the carbon anode S1200 of straw has a good initial reversible capacity, good cycle performance and coulomb efficiency. Therefore, this work provides an efficient, easy to large-scale and environmentally friendly approach for the anodes of sodium-ion cells. It not only meets the requirements of environmental sustainable development, but also can realize the comprehensive utilization of straw resources, creates economic value for the vast number of agricultural farmers in China, and realizes the sustainable development strategy of agricultural crops in China.

Keywords: Sodium-ion batteries, Carbonize temperature, Good cycle performance, Environmentally friendly

1. INTRODUCTION

As traditional fossil fuel supplies dwindle, prices rise, and the gas emissions produced by combustion not only contaminate urban air and contribute to global warming, but also pose a threat to human society's long-term viability. Batteries are one of the most efficient energy storage devices

among the various energy storage systems. Due to high energy density, high power, environmental friendliness, and other advantages, lithium-ion secondary batteries have been widely used in a variety of areas since their introduction, capturing a large market share. Its safe, dependable, robust, and efficient performance is primarily employed in portable electronic devices [1-3], but it may also be used to electrify autos and maintain the stable usage of intermittent renewable energy sources such as wind and solar. However, the global distribution of lithium reserves is uneven and extremely limited, and cost issues may severely limit its long-term development. As a result, the research focus of current energy storage technology has shifted to the development of low-cost and resource-rich materials as alternatives to lithium-ion batteries (LIBs) [4,5]. To address this issue, sodium, which is synonymous with lithium and has similar chemical and physical properties to lithium, is the fourth most abundant element on the planet and has been proposed as a potential replacement for lithium in rechargeable battery systems. In recent years, sodium-ion batteries (SIBs) have been widely concerned [6]. It is expected to replace the next-generation energy storage material [7,8] of LIBs due to its low cost and abundant natural resources.

It is well known that graphite has been commercialized as the negative electrode of lithium-ion batteries and has shown excellent electrochemical performance. However, since the ion radius of sodium ions is larger than the ion diameter of lithium ions (Li^+ 0.76a and Na^+ 1.06a) ((0.76 Å for Li^+ and 1.06Å for Na^+), and traditional graphite cannot meet the embedded [9,10] of sodium ions. As a result, there is a lot of interest in developing a cathode material that allows for sodium ion embedding / deembedding while also having a high energy density, good multiplier properties, and stable circulability. More studied sodium electric anode materials primarily include carbon-based materials and metal materials. Metal anodes typically have a high capacity, but during the cycle, there will be a large volume expansion, powder (pulverization), which will affect the cycle performance of the battery but also bring certain safety risks. Carbon-based cathode materials have a high raw material content, a low cost, a simple synthesis process, and a low working potential. As a result, hard carbon with good circulation, high capacity, and low cost is a promising anode, which is more suitable for manufacturing high-performance sodium ion batteries.

Hard carbon is a high temperature, its structure is more complex than long-range order graphite, no order and stacking rules of graphite layer, its structure contains the nano-graphite area, coiled nano-graphite layer, and the hole between the two, which provides a theoretical basis for hard carbon as a negative electrode material for sodium ion batteries. At the same time, many natural organic compounds in nature are good precursors for the preparation of hard carbon materials, and their unique internal form and structure, as well as their excellent thermal stability and electrical conductivity, have made biomass-derived hard carbon the focus of current research. The "house of cards" model is widely used as a model structure in the currently proposed hard carbon structure for studying the mechanism of ion storage. After electrochemical testing, We found that the storage of sodium ions can be divided into two stages: the first stage is the high voltage ramp at the early stage of discharge, at which sodium ions basic adsorption on the surface and defect site, the second stage is sodium adsorption tends to saturated low pressure platform area, sodium ion primarily through embedded nano-graphite layer storage, this mechanism is also known as adsorption-embedded theory [11]. In order to improve the ability of hard carbon materials to store sodium ions, the adsorption of

sodium ions can be promoted by increasing the specific surface area of carbon layers, the number of intercalation layers and the layer spacing, so as to reduce the resistance of sodium ions unembedding.

Due to its versatility and low cost, biomass has been extensively studied among the available hard carbon precursors [12-14]. Furthermore, the environmental and sustainable properties of "green energy" have increased global interest in biomass in [15]. In recent years, some studies have investigated the production of hard carbon by lignocellulosic biomass and used a variety of biomass, including fruit waste and peel [16-22], grain, shell, shell, leaf, and forestry species [23-30], and recently discovered the application of banana peel [31], sugar [32,33], cellulose [34], lignin [35], peat moss [36], lotus [37], and grapefruit peel [38] in battery research.

Previous research has shown that hard carbon can be produced in an inert atmosphere by direct high temperature carbonization of cotton [39], peanut shell [40], and banana peel [41]. Following in the footsteps of previous studies, we used straw as a hard carbon with a fluffy porous structure and cellulose / hemicellulose as a precursor system.

The electrochemical properties of storage were studied after hard carbon materials were prepared using a simple high temperature treatment. The annual straw crop area in China is vast, but the utilization rate is low; a large number of straw with direct open air incineration treatment has resulted in air pollution, farmland quality decline, soil structure damage, and other issues. In light of the harm caused by excessive straw utilization, straw as a precursor of carbon electrode material production conforms to the requirements of environmental sustainable development, and can realize the comprehensive utilization of straw resources, create economic value for agricultural personnel, and realize the need of our country's agricultural crop sustainable development strategy. This is an important potential resource of biomass derived hard carbon. These promising results, as reported for [42], are due to the use of chemical activation steps to form micropores and an increased surface area. These findings imply that straw-derived carbon has a high potential for SIB anode applications. Unfortunately, previous chemical activation necessitated two or more steps of acid and base neutralization. As a result, we hope to develop a more environmentally friendly method of obtaining porous carbonated structures. To make the straw anode, we simply introduced carbonize without any pretreatment. The effects of different carbonization temperatures on the structure and electrochemical properties of straw derived carbon were studied. Carbonized straw at 1200°C has a higher BET surface area ($47.278\text{m}^2\text{ g}^{-1}$), an interlayer spacing of 3.825nm, and a higher capacity (334.75mAh g^{-1}) than straw carbonized at other temperatures. Although straw-derived carbon has a low specific capacity, it can be significantly increased using simple, environmentally friendly synthesis methods. Compared with other biomass derived carbon, this work adopted a lower reaction temperature (lowering industrial costs), achieves 334.75mAh g^{-1} negative capacity without pretreatment, and most importantly, its source is large-scale biomass waste. which can reduce air pollution and generate income for farmers. Without complex pretreatment, a large surface area can be obtained, and no other biomass-derived carbon has been reported, This shows that straw can be used not only for the electrodes of batteries, but also for other energy storage systems (such as capacitors). In order to improve the utilization of straw and reduce the environmental pollution, we should find a new method to improve its electrochemical performance.

Furthermore, unlike other biomass-derived carbon, our work employs a different load quality. As a result, we will not directly compare the electrochemical properties of our carbon with those of other biomass-derived carbon.

2. EXPERIMENTAL

2.1 Material preparation

We use straw to make hard carbon. We put 2g straw (cut to 1cm) into an alumina crucible and placed it in a tubular furnace using an inert nitrogen flow. The carbon precursor was carbonized at 800°C, 1000°C, and 1200°C (designated S800, S1000, and S1200, respectively), fixed at a heating rate of 5°C/min, and kept at each carbonize temperature for 2 hours. Using a mortar, the prepared carbon substance is ground into a black powder.

2.2 Material characterization

Thermal weight analysis (TG, STA449F5, Germany) is tested at a constant heating rate of 10°C/min. The samples were characterized by X-ray diffraction (XRD, RigakuD / MaxIII diffractor, $\lambda = 1.5418\text{\AA}$) and Raman spectroscopy (Roman, Renisaw inVia spectrometer, 514.5nmAr⁺ laser). The sample was analyzed by a field emission scanning electron microscope (SEM, Hitachi-SU8220). At liquid nitrogen (77K) temperature, we measured the specific surface area and pore distribution of N₂ adsorption-desorption by Autosorb-IQ2; the specific surface area was obtained by Brunauer-Emmett-Teller (BET), and structural parameters such as pore volume and average pore diameter were obtained by Barrett-Joyner-Halenda (BJH).

2.3 Electrochemical characterization

The working electrode consisted of 80wt% active material (straw derived carbon), 10wt% acetylene black and 10wt% polyvinylidene fluoride (PVDF) evenly dispersed in N-methyl-2-pyrrolidone (NMP), coated on copper foil using a scraper and then dried in a vacuum oven at 110°C for 12 hours. The prepared electrodes were cut into 12mm diameter circles of 1.5-2mg / cm². The reverse electrode is metal sodium, with glass fiber as the diaphragm. The electrolyte is a 1M NaClO₄ solution of ethylene carbonate / dimethyl carbonate (EC/DEC, volume of 1:1). In an argon-filled glove box, the Type CR2025 button battery was assembled.

The button battery performs constant current charge and discharge test on the battery with different current density on the NEWARE high performance battery test system, with the test voltage range of 0-2.5V. The cyclic voltammetry (CV) test was performed on a CHI604E electrochemical analyzer (Shanghai Chen Hua Instrument Co., Ltd.) at a scanning rate of 0.1mV. Electrochemical impedance spectroscopy (EIS) was performed on a CHI660E electrochemical analyzer (Shanghai Chen

Hua Instrument Co., Ltd.), scanning the frequency from 100kHz to 10mHz with an AC amplitude of 5mV.

3. RESULTS AND DISCUSSION

3.1 Thermogravimetric Analysis

To determine the required process temperature and get a deeper understanding of the carbonize mechanism of straw, thermal weight (TG) analysis was performed (**Figure 1a**). TG data showed that the thermal degradation of straw occurred in several characteristic steps. Below 100 °C, the weight reduction is mainly due to the removal of water, insufficient to cause changes in the material structure. straw is a living material, a lignocellulosic material composed of lignin, cellulose and hemicellulose. The actual carbonization process of straw can be divided into four stages mainly due to water removal, hemicellulose, cellulose and lignin, with the first stage being 0-100°C, the second 100-300°C, the third approaching 300-480°C and the fourth 480-1200°C.

The decomposition temperatures of the three lignocellulose components are as follows: hemicellulose, cellulose and lignin were 210-325°C, 310-400°C and 160-900°C [43], respectively, this is in complete agreement with the results we observed in the experiment. These three lignocellulose contain volatile ethers, alcohols and methyl groups, which evaporate with the increase of carbonization temperature and finally form solid carbon products [44]. The average yields of S800, S1000, and S1200 were 24.9%, 24.4%, and 23.8%, respectively, which coincided with the thermal weight theoretical values.

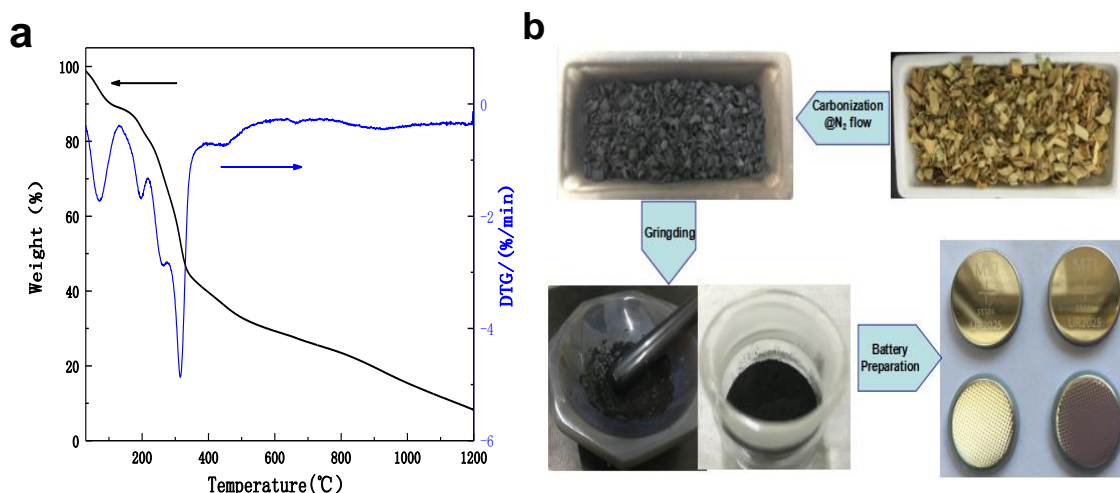


Figure. 1 a) TG results of straw in inert atmosphere N₂. b) rechargeable SIBs was prepared with straw at 800°C, 1000°C and 1200°C

3.2 Carbon Morphology Analysis of Straw

The microstructure of straw derived carbon prepared at different temperatures was studied by field emission scanning electron microscope. In a, b and c, **Figure 2** shows straw-derived hard carbon

in all samples. It can be seen that the size of hard carbon particles is not uniform, smooth surface, fewer pores, and some small hard carbon particles are attached to the surface of large particles. However, the morphology and size of carbon particles are very similar. As the decomposition temperature increased, we found that the carbon content of all straw derived carbon increased and the oxygen content decreased, as shown in **Figure 2**.

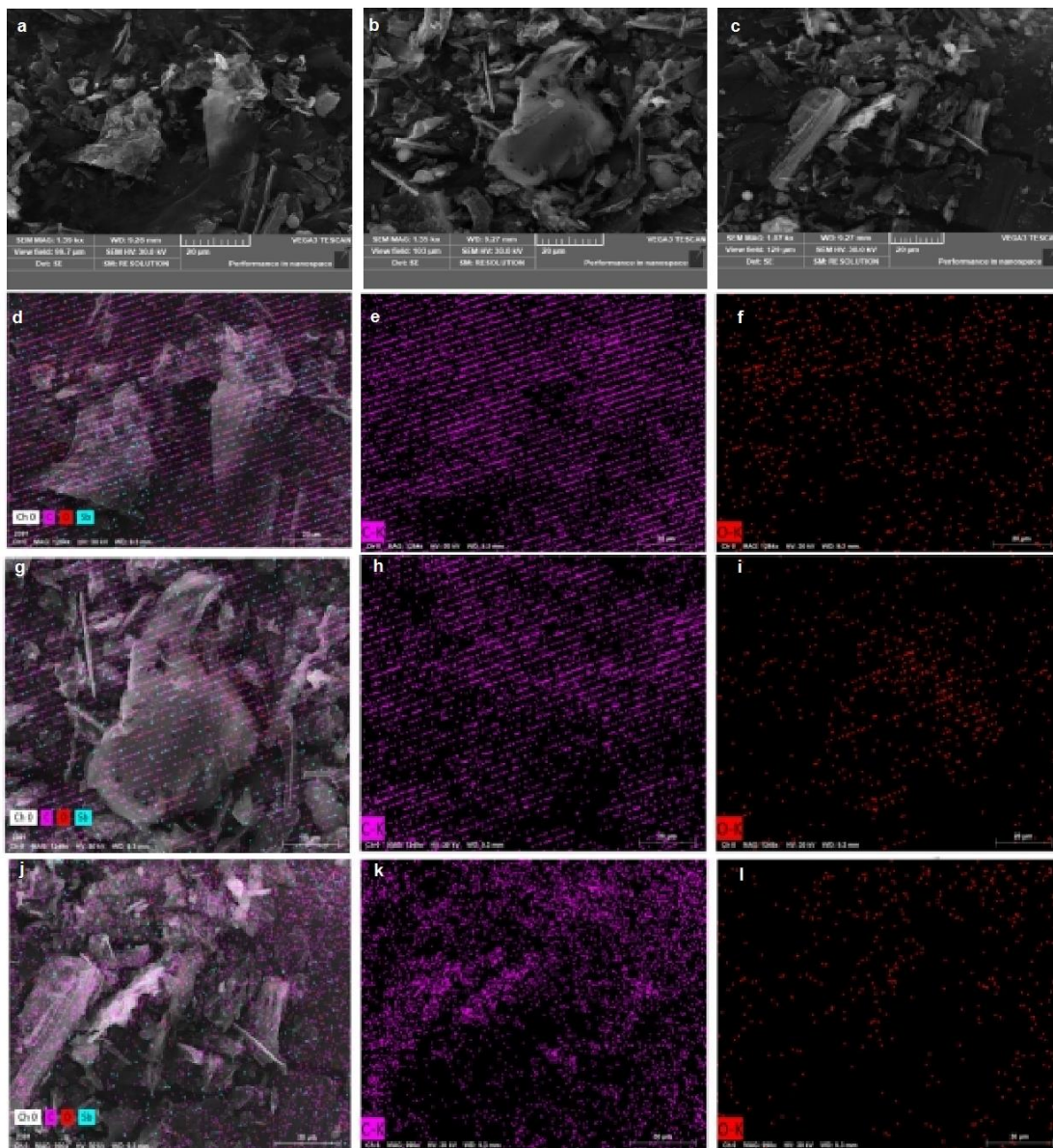


Figure 2. SEM map and element map of carbon derived from straw: a). SEM map of S800; b). S1000; c). S1200. d), e), f). S800. g), h), i). S1000; and j), k), l). S1200 corresponding elements mapping.

3.3 Structural Analysis of Straw Derived Carbon by XRD and Raman Spectroscopy

X-ray Diffraction (XRD) mapping and Raman spectral analysis were first performed and the results are shown in **Figure 3a** shows the XRD pattern of straw-derived carbon prepared at different

temperatures, with two peaks observed at 23 and 43, namely (002) and (100). Furthermore, the (002) peak position turn round a low angle as the carbon temperature increases, it indicates that the high temperature increases the interlayer distance (d_{002}). The Raman spectra have two significant peaks at $\sim 1358\text{cm}^{-1}$, and $\sim 1592\text{cm}^{-1}$, respectively related to the band D (sp^2 carbon atoms with disordered and defective conditions) and the G band (carbon atoms in a flat sp^2 configuration). The half-width of the G and D bands decreases at the half-maximum as the carbide temperature increases, The development of local short-range ordered structures is further clarified [45-47]. This result is consistent with the previous report.

Structural studies of straw derived carbon were performed by XRD and Roman. Figure 3a shows the XRD profiles of S800, S1000, and S1200. It can be observed from the figure that straw derived carbon materials prepared at different temperatures have two broad diffraction peaks, corresponding to graphite lattice reflection peak (002) and reflection peak (100), which are typical amorphous carbon materials. The diffraction angle 2θ of the corresponding reflection peak (002) is 21.74, 21.90 and 26.63, respectively, and the diffraction angle 2θ of the corresponding reflection peak (100) is 41.96, 42.38 and 45.40, respectively. As the carbonize temperature increases, the peak (002) position moves to a low angle, indicating that the high temperature will increase the interlayer distance between the graphite sheets (002).

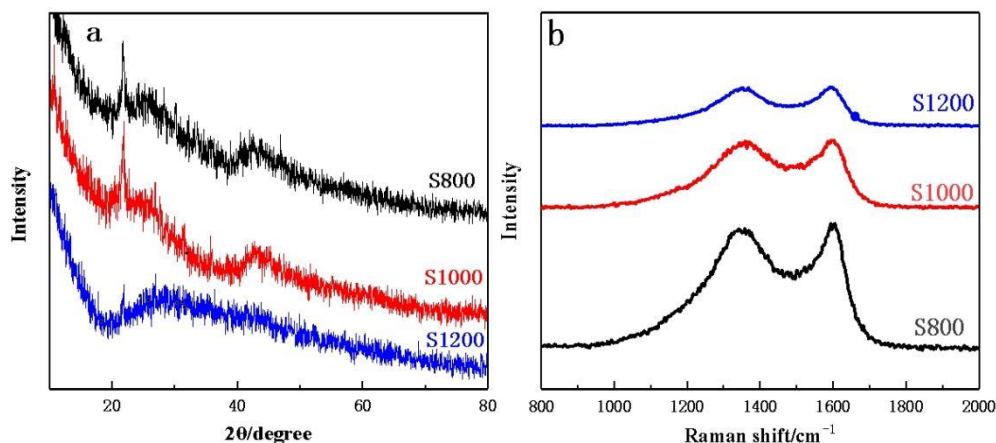


Figure 3. Characterization of the carbonize reaction of carbon derived from straw at different temperatures: a) XRD patterns. b) Raman spectra.

In order to further understand the graphitization degree of straw derived carbon prepared at different temperatures, we performed Raman spectroscopy of these three hard carbon materials. From **Figure 3b**, the three straw derived carbon materials have two Raman absorption peaks near 1350cm^{-1} and 1580cm^{-1} , corresponding graphite structure defects, amorphous carbon sp^3 carbon vibration D peak (D peak represents disorder, defective carbon content in carbon material) and sp^2 hybrid graphite carbon vibration G peak (G peak value represents the carbon graphite, the value of the G peak, the higher, the better the overall conductivity of the composite material.) With the increase of carbonization temperature, the half width of G-band and D-band decreases and the diffraction peaks

become sharper, which further clarifies the better [48] for the development of local short-range ordered structures. The results of Raman spectrum analysis and XRD data are consistent with the report [31].

3.4 N_2 adsorption desorption characterization of straw derived carbon

To further study the pore structure, we used N_2 adsorption desorption to measure the pore distribution and specific surface area. The specific surface area of material by Brunauer-Emmett-Teller (BET) and structural parameters such as pore distribution, average pore diameter and pore volume were tested at 77k by Barrett-Joyner-Halenda (BJH). The isothermal adsorption detachment curve of nitrogen in the sample was obtained by measuring the nitrogen adsorption / D. ($P / P_0 = 10^{-7} \sim 0.99$). The sample was pretreated before the BET adsorption detachment experiment, that is, vacuum degassing for 5h at 150°C to remove impurities such as water vapor in the sample.

The N_2 adsorption-desorption isotherm can directly reflect the pore structure changes of the hard carbon material, and calculation of specific surface area and pore structure. Fig. 4 shows the N_2 adsorption desorption isotherms and corresponding pore distribution of three straw derived carbons. The BET surface area of S800, S1000, and S1200 is $37.780\text{m}^2\text{g}^{-1}$, $41.578\text{m}^2\text{g}^{-1}$ and $47.278\text{m}^2\text{g}^{-1}$, respectively. The BET surface area increased with the preparation temperature, which can be attributed to lignin decomposition, which ranges from 210 to 900°C as previously described. Thus, the lignin breakdown was better achieved at 1200°C than done at 800°C and 1000°C , which may explain the higher surface area of S1200.

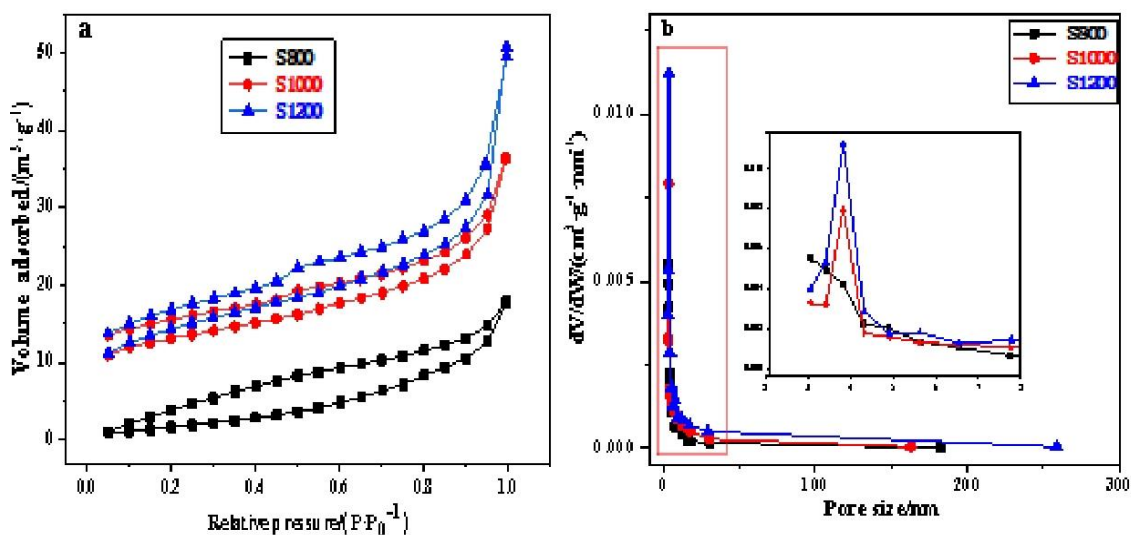


Figure 4. a) N_2 adsorption-desorption isothermal curves. b) BJH pore diameter distribution curve

From the BJH pore distribution curve, it can be seen that the straw derived carbon prepared at different temperatures shows very similar pore distribution characteristics, with its pore size mainly distributed between 2.5 and 15nm, but has different pore volumes at different pore diameter positions,

where S1200 shows the maximum pore volume of $0.056\text{cm}^3\text{g}^{-1}$ and the maximum average pore diameter of 3.825nm . These mesopholes should come from the void [49-52] generated by the accumulation of pyrolytic carbon nanoparticles. Table 1 further gives BJH pore structure and the BET specific surface area data of straw derived carbon materials prepared at different temperatures.

Table 1. Specific surface area and BJH pore diameter structure of straw derived carbon materials prepared at different temperatures

| Sample | BET surface area/ ($\text{m}^2\cdot\text{g}^{-1}$) | Total pore volume/ ($\text{cm}^3\cdot\text{g}^{-1}$) | The average pore diameter/nm |
|--------|---|---|------------------------------|
| S800 | 37.780 | 0.024 | 3.058 |
| S1000 | 41.578 | 0.037 | 3.822 |
| S1200 | 47.278 | 0.056 | 3.825 |

3.5 Electrochemical Characterization

A button half battery was first used to test the electrochemical properties of straw-derived carbon samples. **Figures 5a-c** show the first two cycle voltampere curves CV (Cyclic voltammetry) of S800, S1000 and S1200 straw derived carbon electrodes at 0.1mV S^{-1} with the voltage window value of 0-2.5V, a scanning rate of 0.1mV S^{-1} and a voltage interval of 0-2.5V vs. Na^+/Na . Comparing the test results of S800, S 100, S1000 and S1200, S1200 shows that S 1200 has two reduction peaks at 0.75V, similar to the electrochemical reaction of other carbon materials.

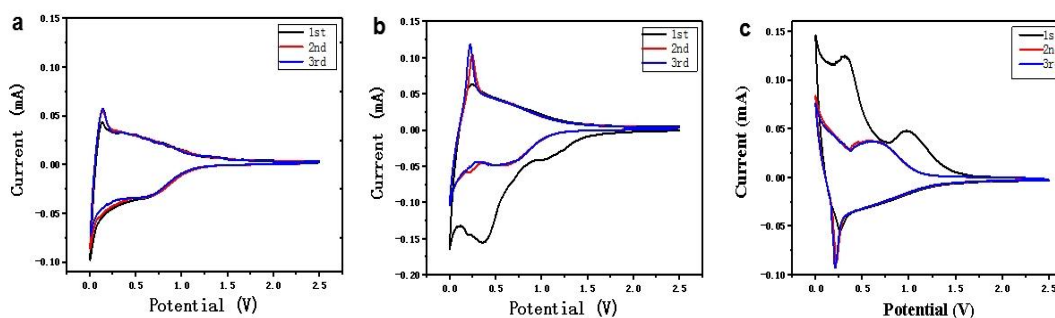


Figure 5. Electrochemical measurements of straw derived carbon samples. a,b,c are the CV curves of S800, S1000, and S1200, respectively

There is a pair of sharp oxidation / reduction peaks at 0.1V indicates straw derived carbon formation due to the insertion of Na^+ into the intermediate [53-54] formed between the hard carbon layer. This is related to the oxidation / reduction of straw derived carbon, the reduction peak corresponds to the decomposition of electrolyte reduction and the production of SEI (Solid-electrolyte

Interphase) membrane; the next wide peak centered at 0.75V is due to the irreversible capture of sodium ions into high active defects, electrolyte decomposition and SEI membrane formation and reduction reaction. In addition to the first loop curve, the shape and size are extremely similar, and the second loop of the peak also overlap well, indicating that the generated SEI film can be stably present on the surface of the electrode and has good Na⁺ storage activity, proving that S1200 straw derived carbon material has good reversible properties. **Figure 6** depicts the constant current charge and discharge curve, multiplier performance, cycle performance, and Coulomb efficiency. The first loop charge-discharge graph at **Figure 6a** current density of 50mA g⁻¹ clearly shows two distinct phases. The first stage is a 2.5-1.0V tilted region caused through the adsorption of Na⁺ on the defect position, edge and surface of the nano graphite domain. The second feature is the platform area below 1.0V, which is attributed to Na⁺ insertion into the graphite-like microcrystal line[55]. In practice, the low-voltage platform will aid in increasing the overall energy density of the battery.

The fold performance is shown in **Figure 6b**. The current densities of S800, S1000 and S1200 begin to increase and return to their initial values at 50mA g⁻¹, and it is clearly observed that S1200 exhibits better stability over a larger range of working current densities. S1200 provides capacities of 334.705, 182.38, 144.56, 57.85 and 43.36mAh g⁻¹ at 50, 150, 300, 900, 1500 mA g⁻¹, respectively, S800 and S1000 have similar fold performance. Furthermore, all carbon electrodes had a poor capacity at a current density of 1500mA g⁻¹, This is consistent with the reported studies [56,57]. The insufficient capacity at high current density is due to its own resistance, resulting in overpotential, prompting the half battery to reach the cutoff voltage of [58,59] early before full saturation.

The cycling properties of different straw derived carbon electrodes were measured by constant current charge and discharge, as shown in **Figure 6c**, with initial reversible capacities of S800, S1000 and S1200 and 252.98mAh g⁻¹ at 50mA g⁻¹, respectively. After 75 cycles, the reversible capacities of S800, S1000 and S1200 remained at 147.75, 146.13 and 206.93mAh g⁻¹, and in all samples S1200 had not only the highest reversible capacity but also good cycle stability, although the reversible capacity was reduced to about 240.27mAh g⁻¹ in the second cycle. When the electrode runs for 75 cycles at 50mA g⁻¹, the capacity remains at 206.93mAh g⁻¹, with a capacity retention rate of 81.8%. In contrast, the capacity retention rates of the S800 and S1200 were 55.23% and 77.29% after 75 cycles, respectively. The first Coulomb efficiencies of S800, S1000 and S1200 were 87.9%, 94.7% and 93.3%, respectively, but it is clear from the figure that S1200 remained above 99% for S1000 and S800 for S1000 remained above 98%. Therefore, the S1200 carbon electrode has high reversible capacity and has good cycle stability energy and coulomb efficiency.

We used EIS analysis to better analyze the electrochemical properties of straw derived carbon, as shown in **Figure 6d**. After 5 cycles, the half-cell was measured at a current density of 50mAh g⁻¹. The Nyquist diagram clearly shows that it is made up of individual semicircle slope curves and low frequency region. The diameter of the semicircle indicates the charge transfer resistance (RCT) between the carbon electrode and the electrolyte in the medium and high frequency range, and the low-frequency slope indicates the solid diffusion of sodium ions in the active material, indicating the Warburg impedance. The S1200 carbon electrode clearly has the smallest Rct of all samples, indicating that S1200 material has higher conductivity and easier charge transfer.

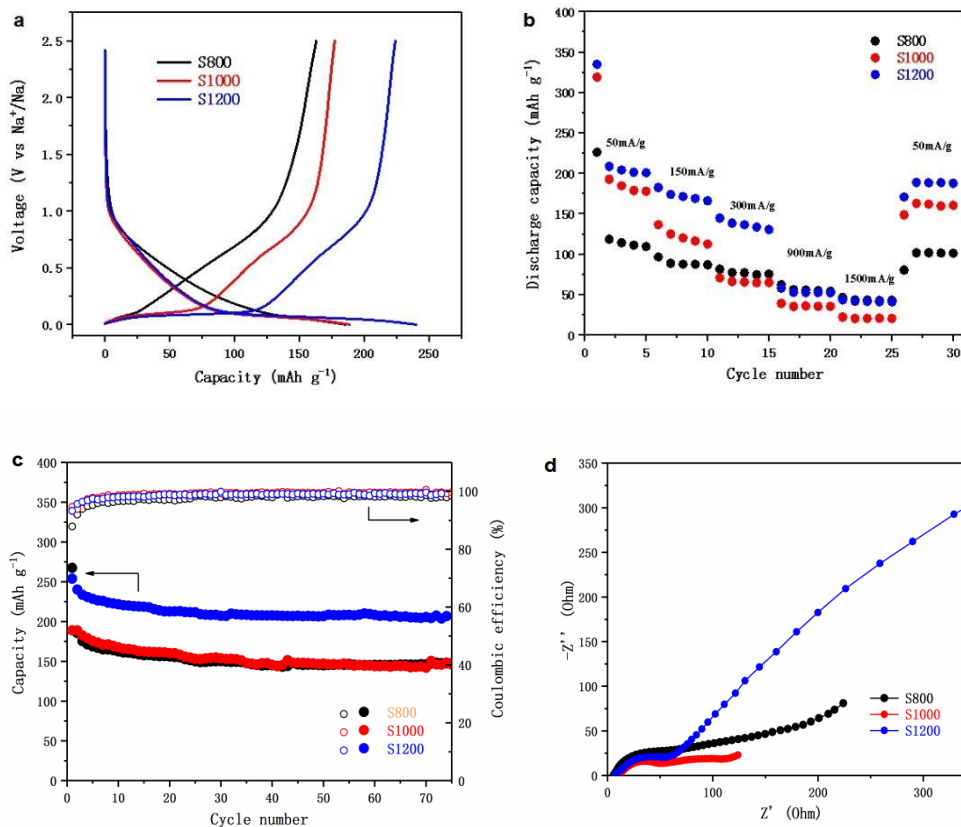


Figure 6. Electrochemical properties of straw derived carbon at different temperatures: a) The first-cycle charge and discharge profiles at a current density of 50 mA g^{-1} ; b) The rate performance at different current densities; c) The cycling capacity and the coulomb efficiency at 50 mA g^{-1} ; d) Post-impedance map for 5 cycles of S 800, S1000, and S1200 electrodes at 50 mA g^{-1} .

Table 2. The sodium storage capacities of HC derived from different precursors

| Precursor | TT (°C) | Reversible capacity | Ref |
|------------------|---------|---|-----------|
| Cotton | 1300 | 315 mAh g^{-1} at 30 mA g^{-1} | 60 |
| Corn cobs | 1300 | 298 mAh g^{-1} at 30 mA g^{-1} | 61 |
| Peanut shell | 1300 | 299 mAh g^{-1} at 0.1C | 62 |
| Kelp | 1300 | 334 mAh g^{-1} at 25 mA g^{-1} | 63 |
| Kapok fiber | 1400 | 290 mAh g^{-1} at 30 mA g^{-1} | 64 |
| Lignin | 1300 | 328 mAh g^{-1} at 50 mA g^{-1} | 65 |
| Tamarind | 1200 | 326.7 mAh g^{-1} at 50 mA g^{-1} | 66 |
| Blue-green algae | 1000 | 230 mAh g^{-1} at 20 mA g^{-1} | 67 |
| S1200 | 1200 | $334.75 \text{ mAh g}^{-1}$ at 50 mA g^{-1} | This Work |

This will be more beneficial in terms of improving the multiplier performance and cycle performance of the S1200 electrodes, which is consistent with the earlier conclusions.

In conclusion, the 1200°C straw-derived carbon electrode S1200 outperforms the S800 and S1000 in terms of charge and discharge performance, reversible capacity, cycle stability, and coren efficiency. It can be fully explained that the carbonize temperature of the carbon electrode is the primary determinant of the electrochemical behavior during sodium storage.

All in all, if one compares the sodium storage capacities with the results reported in the literature (Table 2), one can notice that S1200 show better electrochemical performance, and have the advantages of raw materials being commercially available.

4. CONCLUSION

By using a simple carbonize method, a series of carbon electrode materials were created. The best electrochemical properties were found in straw fibers carbonized at 1200°C. The initial reversible capacity of the S1200 is 334.75mAh g⁻¹. When the electrode is operated at 50 mA g⁻¹, the capacity can be maintained at 206.93mAh g⁻¹, the capacity retention rate is 81.8 percent, and the coulomb efficiency of the first circle is 93.3%, indicating that it has good cycle performance and has high research value for the commercialization of SIBs. The main determinant of the electrochemical behavior during sodium storage is the carbonize temperature of the carbon electrodes. This study offers a cost-effective and environmentally friendly method for producing carbon electrode materials for energy storage, as well as reasonable guidance for the preparation of precursors.

ACKNOWLEDGMENTS

This research was financially supported by the project of trategic Cooperation Project of Luzhou Municipal People's Government of Sichuan University (2020CDLZ-20); Luzhou City key science and technology projects(2019-NYF-28) and Institute-level Project of Sichuan Vocational College of Chemical Technology (SCHYA-2022-06). Thanks to the School of Chemical Engineering of Sichuan University, the High Research Institute of Sichuan University, and the School of Materials and Chemical Engineering of Sichuan Light Chemical Engineering University for their help in the whole experiment.

References

1. B. Dunn, H. Kamath and J. Tarascon, *Science*, 334 (2011) 928.
2. P. Bruce, B. Scrosati and J. Tarascon, *Angew. Chem., Int. Ed.*, 47 (2008) 2930.
3. H. Pan, Y. Hu and L. Chen, *Energy Environ. Sci.*, 6 (2013) 2338.
4. L. Su, Y. Jing and Z. Zhou, *Nanoscale*, 3 (2011) 3967.
5. Y. Zhong, M. Yang, X. Zhou, Y. Luo, J. Wei and Z. Zhou, *Adv. Mater.*, 27 (2015) 809.
6. M.D. Slater, D. Kim, E. Lee and C.S. Johnson, *Adv. Mater.*, 23 (2013) 958.
7. Y.E. Zhu, X. Qi, X. Chen, X. Zhou, X. Zhang, J. Wei, Y. Hu and Z. Zhou, *J. Mater. Chem. A*, 4 (2016) 11106.
8. X. Zhou, Y. Zhong, M. Yang, M. Hu, J. Wei and Z. Zhou, *Chem. Commun.*, 50 (2014) 12888.
9. M.D. Slater, D. Kim, E. Lee and C.S. Johnson, *Adv. Funct. Mater.*, 23 (2013) 947.
10. M. Dahbi, N. Yabuuchi, K. Kubota, K. Tokiwa and S. Komaba, *Phys. Chem. Chem. Phys.*, 16 (2014) 15013.
11. Y. Zhang, X. Li and P. Dong, *ACS Appl. Mater. Interfaces*, 10 (2018) 42803.

12. H. Hou, X. Qiu and W. Wei, *Adv. Energy Mater.*, 7 (2017) 1602898.
13. C.D.M.S. Rios, V. Simone, L. Simonin, S. Martinet and C. Dupont, *Biomass Bioenergy*, 117 (2018) 35.
14. N. Zhang, Q. Liu, W. Chen, M. Wan, X. Li, L. Wang, L. Xue and W. Zhang, *J. Power Sources*, 378 (2018) 336.
15. T. Zhang, J. Mao, X. Liu, M. Xuan, K. Bi, X.L. Zhang, J. Hu, J. Fan, S. Chen and G. Shao, *RSC Adv.*, 7 (2017) 41507.
16. L. Wu, D. Buchholz, C. Vaalma, G.A. Giffiffiffin and S. Passerini, *ChemElectroChem*, 3 (2016) 295.
17. I. Izanar, M. Dahbi, M. Kiso, S. Doubaji, S. Komaba and I. Saadoune, *Carbon*, 137 (2018) 169.
18. Y. Zhu, M. Chen, Q. Li, C. Yuan and C. Wang, *Carbon*, 129 (2018) 699.
19. K. Wang, Y. Jin, S. Sun, Y. Huang, J. Peng, J. Luo, Q. Zhang, Y. Qiu, C. Fang and J. Han, *ACS Omega*, 2 (2017) 1689.
20. S. Talekar, A.F. Patti, R. Vijayraghavan and A. Arora, *ACS Sustainable Chem. Eng.*, 6 (2018) 16370.
21. J. Xiang, W. Ling, C. Mu, J. Zhao and B. Wang, *J. Alloys Compd.*, 701 (2017) 872.
22. E.M. Lotfabad, J. Ding, K. Cui, A. Kohandehghan, W.P. Kalisvaart, M. Hazelton and D. Mitlin, *ACS Nano*, 8 (2014) 7122.
23. S.D. Xu, Y. Zhao, S. Liu, X. Ren, L. Chen, W. Shi, X. Wang and D. Zhang, *J. Mater. Sci.*, 53 (2018) 12334.
24. K. Kim, D.G. Lim, C.W. Han, S. Osswald, V. Ortalan, J.P. Youngblood, V.G. Pol, *ACS Sustainable Chem. Eng.*, 5 (2017) 8720.
25. X. Ren, S.D. Xu, S. Liu, L. Chen, D. Zhang and L. Qiu, *E. Chem.*, 841 (2019) 63.
26. W. Lv, F. Wen, J. Xiang, J. Zhao, L. Li, L. Wang, Z. Liu and Y. Tian, *J. Electroanal. Chem.*, 176 (2015) 533.
27. M. Dahbi, M. Kiso, K. Kubota, T. Horiba, T. Chafifik, K. Hida, T. Matsuyama and S. Komaba, *J. Mater. Chem. A*, 5 (2017) 9917.
28. S. Zhang, Y. Li and M. Li, *JOM.*, 70 (2018) 1387.
29. Q. Wang, X. Zhu, Y. Liu, Y. Fang, X. Zhou and J. Bao, *Carbon*, 127 (2018) 658.
30. L. Cao, W. Hui, Z. Xu, J. Huang, P. Zheng, J. Li and Q. Sun, *J. Alloys Compd.*, 695 (2017) 632.
31. P. Kalyani, and A. Anitha, *Int. J. Hydrogen Energy*, 38 (2013) 4034.
32. E. M. Lotfabad, Lotfabad E M, Ding J and Cui K, *ACS Nano*, 8 (2014) 7115.
33. W. B. Xing, R. A. Dunlap and J. R. Dahn, *J. Electrochem. Soc.*, 145 (1998) 62.
34. S. Babu R and M. Pyo, *J. Electrochem. Soc.*, 161 (2014) A1045.
35. F. Shen, H. Zhu and W. Luo, *ACS Appl. Mater. Interfaces*, 7(2015)23291.
36. J. Jin, S.J. Yu, Z.Q. Shi, C.Y. Wang and C.B. Chong, *J. Power Sources*, 272 (2014) 805.
37. J. Ding, H. Wang and Z. Li, *Acs Nano.*, 7 (2013) 11004.
38. P. Wang, B. Qiao and Du Y, *J. Phys. Chem. C*, 119 (2015) 21336.
39. K.L. Hong, L. Qie and R. Zeng, *J. Mater. Chem. A*, 2(2014)12733.
40. Y. Li, Y. Hu, M. Titirici, L. Chen and X. Huang, *Adv. Energy Mater.*, 6(2016)1600659.
41. J. Ding, H. Wang, Z. Li, K. Cui, D. Karpuzov, X. Tan, A. Kohandehghan and D. Mitlin, *Energy Environ. Sci.*, 8(2015)941.
42. J. Xu, Q. Gao and Y. Zhang, *Sci. Rep.*, 4(2014)1.
43. K. C. Kil and U. Paik, *Macromol. Res.*, 23(2015)719.
44. A. C. Lua and T. Yang, *J. Colloid Interface Sci.*, 276(2004)364.
45. J. Ding, H. Wang, Z. Li, A. Kohandehghan, K. Cui, Z. Xu, B. Zahiri, X. Tan, E. Lotfabad, B. Olsen and D. Mitlin, *ACS Nano*, 7(2013)11004.
46. P. Liu, Y. Li, Y. Hu, H. Li, L. Chen and X. Huang, *J. Mater. Chem. A*, 4(2016)13046.
47. A. Ferrari, J. Meyer, V. Scardaci, C. Casiraghi, M. Lazzeri, F. Mauri and S. Piscanec, *Phys. Rev. Lett.*, 97(2006)187401.

48. Y. Li, Y. Hu, H. Li, L. Chen and X. Huang, *J. Mater. Chem. A*, 4(2016)96.
49. X. L. Wu, L. L. Chen, S. Xin, Y. X. Yin, Y. G. Guo, Q. S. Kong and Y. Z. Xia, *ChemSusChem*, 3 (2010)705.
50. X.L. Wu, W. Wang, Y.G. Guo and L.J. Wan, *J. Nanosci. Nanotechnol.*, 11(2011)1897.
51. Y.Y. Wang, B.H. Hou, H.Y. Lu, C.L. Lu, X.L. Wu, *ChemistrySelect*, 1 (2016)1441.
52. Y.Y. Wang, B.H. Hou, H.Y. Lu, F. Wan, J. Wang, and X.L. Wu, *RSC Adv.*, 5 (2015)97427.
53. F. Qi, Y. Chen and B. Zheng, *J. Mater. Sci.*, 52 (2016)3622.
54. Y. Liu, H. Kang and L. Jiao, *Nanoscale.*, 7 (2015)1325.
55. X. Cao, Y. Shi and W. Shi, *Small*, 9 (2013) 3433.
56. Y. Li, Y. S. Hu, M. M. Titirici, L. Chen and X. Huang, *Adv. Energy Mater.*, 6(2016)1600659.
57. F. Xie, Z. Xu, A.C. Jensen, F. Ding, H. Au, J. Feng and H. Luo, *J. Mater. Chem. A*, 7(2019)27567.
58. H. Au, H. Alptekin, A. Jensen, E. Olsson, C.A. O'Keefe and T. Smith, *Energy Environ. Sci.*, 8(2020)3469.
59. Z. Li, Z. Jian, X. Wang, I.A. Rodriguez-Perez, C. Bommier and X. Ji, *Chem. Commun.* 53(2017)2610.
60. Y. Li, Y.S. Hu, M.M. Titirici, L. Chen and X. Huang, *Adv. Energy Mater.*, 6 (2016) 1600659.
61. P. Liu, Y.M. Li, Y.S. Hu, H.Li, L.Q. Chen and X.J. Huang, *J. Mater. Chem. A*, 4(2016)13046.
62. X.W. Dou, I. Hasa, M. Hekmatfar, T. Diemant, R.J. Behm and D. Buchholz, *ChemSusChem*, 10(2017)2668.
63. P.Z. Wang, X.S. Zhu, Q.Q. Wang, X. Xu, X.S. Zhou and J.C. Bao, *J. Mater. Chem. A*, 5(2017)5761.
64. Z.E. Yu, Y.C. Lyu, Y.T. Wang, S.Y. Xu, H.Y. Cheng and X.Y. Mu, *Chem. Commun.*, 56(2020)778.
65. S. Alvin, C. Chandra and J. Kim, *Chem. Eng. J.*, 391(2019)123576.
66. K.H. Yu, H.C. Zhao, X.R. Wang, M.H. Zhang, R.Q. Dong and Y. Li, *ACS Appl. Mater. Interfaces*, 12 (2020) 10550.
67. X. Meng, P.E. Savage and D. Deng, *Environ. Sci. Technol.*, 49(2015)12545.